Journal of The Electrochemical Society

Electrochemistry of Titanium and the Electrodeposition of Al-Ti Alloys in the Lewis Acidic Aluminum Chloride – 1-Ethyl-3-methylimidazolium Chloride Melt

Tetsuya Tsuda, Charles L. Hussey, Gery R. Stafford and John E. Bonevich

J. Electrochem. Soc. 2003, Volume 150, Issue 4, Pages C234-C243.
doi: 10.1149/1.1554915

Email alerting service Receive free email alerts when new articles cite this article - sign up in the box at the top right corner of the article or click here

To subscribe to *Journal of The Electrochemical Society* go to:
http://jes.ecsdl.org/subscriptions

© 2003 ECS - The Electrochemical Society

Downloaded on 2012-10-05 to IP **128.143.23.241** address. Redistribution subject to ECS license or copyright; see **www.esltbd.org**

Journal of The Electrochemical Society, **150** (4) C234-C243 (2003)
0013-4651/2003/150(4)/C234/10/$7.00 © The Electrochemical Society, Inc.

Electrochemistry of Titanium and the Electrodeposition of Al-Ti Alloys in the Lewis Acidic Aluminum Chloride–1-Ethyl-3-methylimidazolium Chloride Melt

Tetsuya Tsuda,[a,*] Charles L. Hussey,[a,*,z] Gery R. Stafford,[b,*] and John E. Bonevich[b]

[a]*Department of Chemistry and Biochemistry, The University of Mississippi, University, Mississippi 38677, USA*
[b]*National Institute of Standards and Technology, Materials Science and Engineering Laboratory, Gaithersburg, Maryland 20899, USA*

The chemical and electrochemical behavior of titanium was examined in the Lewis acidic aluminum chloride-1-ethyl-3-methylimidazolium chloride ($AlCl_3$-EtMeImCl) molten salt at 353.2 K. Dissolved Ti(II), as $TiCl_2$, was stable in the 66.7-33.3% mole fraction (m/o) composition of this melt, but slowly disproportionated in the 60.0-40.0 m/o melt. At low current densities, the anodic oxidation of Ti(0) did not lead to dissolved Ti(II), but to an insoluble passivating film of $TiCl_3$. At high current densities or very positive potentials, Ti(0) was oxidized directly to Ti(IV); however, the electrogenerated Ti(IV) vaporized from the melt as $TiCl_4(g)$. As found by other researchers working in Lewis acidic $AlCl_3$-NaCl, Ti(II) tended to form polymers as its concentration in the $AlCl_3$-EtMeImCl melt was increased. The electrodeposition of Al-Ti alloys was investigated at Cu rotating disk and wire electrodes. Al-Ti alloys containing up to ~19% atomic fraction (a/o) titanium could be electrodeposited from saturated solutions of Ti(II) in the 66.7-33.3 m/o melt at low current densities, but the titanium content of these alloys decreased as the reduction current density was increased. The pitting potentials of these electrodeposited Al-Ti alloys exhibited a positive shift with increasing titanium content comparable to that observed for alloys prepared by sputter deposition.
© 2003 The Electrochemical Society. [DOI: 10.1149/1.1554915] All rights reserved.

Manuscript submitted July 23, 2002; revised manuscript received September 30, 2002. Available electronically February 28, 2003.

The resistance of aluminum to chloride-induced pitting corrosion can be improved significantly by alloying with transition metals such as Cr, Cu, Mo, Mn, Nb, Ta, Ti, V, and Zr and rare earths such as Er and Ce. However, improved corrosion resistance is not observed unless these solutes are present at concentrations greatly exceeding their normal equilibrium solubilities, which in most cases is less than 1% atomic fraction (a/o). This is because the pitting potential of aluminum is often related directly to the solute concentration, with greater concentrations leading to increased corrosion resistance.[1,2] However, if the solute metal forms a precipitate, then the corrosion resistance of the aluminum is reduced because the precipitated solute forms microgalvanic corrosion cells.[3] Thus, nonequilibrium alloying methods such as rapid solidification or melt spinning,[4,5] ion implantation,[6-9] reactive plasma spraying,[10,11] sputter deposition,[3,12-16] and thermal evaporation[17] are needed in order to prepare single-phase materials. However, a more advantageous method for producing these alloy films is electrodeposition because this approach can lead to alloy coatings of uniform composition and structure.

Titanium is one of several transition elements that have been found to improve the corrosion resistance of aluminum.[13] The electrochemistry of titanium has been studied extensively in Lewis acidic chloroaluminate melts,[18-24] and it has been determined that Al-Ti alloys can be electrodeposited from solutions of Ti(II) in these melts.[20-24] In 66.7-33.3% mole fraction (m/o) $AlCl_3$-NaCl melt at 423 K, Al-Ti alloys containing up to 28 a/o titanium were obtained by varying the Ti(II) concentration and/or the applied current density.[20,21] However, when the Ti(II) concentration was raised above 150 mmol L^{-1} in this melt at this temperature, the titanium content of the alloy became virtually independent of the current density, and $TiAl_3$, with an ordered $L1_2$ crystal structure was produced.

In this article, we report the electrochemistry of titanium in the Lewis acidic $AlCl_3$-1-ethyl-3-methylimidazolium chloride ($AlCl_3$-EtMeImCl) molten salt at 353.2 K as it pertains to the electrodeposition of Al-Ti alloys. The aim of this study is to clarify the effects of the melt composition, Ti(II) concentration, and hydrodynamic transport rate on the Al-Ti alloy composition and to determine the best route for introducing Ti(II) into the electroplating bath.

Experimental[a]

The procedures used for the synthesis of EtMeImCl, the purification of $AlCl_3$ by sublimation, and the preparation and purification of the $AlCl_3$-EtMeImCl molten salt were identical to those described in previous articles.[25,26] Anhydrous titanium (II) chloride (Aldrich, 99.98%) and anhydrous titanium (III) chloride (Aldrich, 99.999%) were used as received. Titanium (IV) chloride (Matheson, Coleman, & Bell, 99.5%) was used after dehydration. All molten salt experiments were carried out in a nitrogen gas-filled glove box (VAC Atmospheres NEXUS system) with O_2 and $H_2O < 5$ ppm. Molten salt voltammetry experiments were conducted by using a Pine Instruments Co. model AFCBP1 bipotentiostat controlled with PineChem for Windows software running on a microcomputer. The anodic polarization of a titanium wire working electrode and the electrodeposition of Al-Ti alloy were performed with an EG&G PARC model 173 potentiostat/galvanostat equipped with a model 179 digital coulometer plug-in module. Potentiodynamic pitting corrosion measurements were carried out with an EG&G PARC model 263 potentiostat/galvanostat.

All electrochemical experiments were conducted in three-electrode cells. For experiments in the molten salt, the working electrode was either a Pine Instruments Teflon-sheathed platinum rotating disk electrode (geometrical area = 0.099 cm^2), a length of 0.5 mm diam titanium wire (Alfa Aesar, 99.98%), or a small disk electrode prepared by sealing a length of the aforementioned titanium wire in a Pyrex glass tube and cutting off the end of the sealed tube so as to expose the cross section of the wire. Coils of 1.0 mm diam aluminum wire (Alfa Aesar, 99.999%) were used for the counter and reference electrodes. These electrodes were immersed in a melt with the same composition as the bulk melt, but were separated from the bulk melt by a porosity *E* glass frit (Ace Glass). The aluminum electrodes were cleaned with a mixture of concentrated H_2SO_4,

* Electrochemical Society Active Member.
z E-mail: chclh@chem1.olemiss.edu

[a] Certain trade names are mentioned for experimental information only; in no case does it imply a recommendaion or endorsement by NIST.

Downloaded on 2012-10-05 to IP 128.143.23.241 address. Redistribution subject to ECS license or copyright; see www.esltbd.org

HNO_3, and H_3PO_4, rinsed with distilled H_2O, and dried under vacuum before use.

Alloy samples of approximately 10 μm thickness were electroplated from solutions of Ti(II) in the $AlCl_3$-EtMeImCl molten salt onto a length of 1.25 mm diam copper wire or a copper disk (geometrical area = 0.80 cm^2). The elemental composition of each sample was determined by energy dispersive X-ray (EDX) spectroscopy. Potentiodynamic pitting corrosion measurements were carried out on these alloy samples at room temperature in a 0.1 mol L^{-1} solution of NaCl in distilled H_2O. This solution was deaerated with nitrogen gas before each experiment. The reference electrode for these measurements was a sodium-saturated calomel electrode (SSCE), and the counter electrode was a large surface area platinum wire coil. A known length of the plated Cu wire was exposed to the NaCl solution by using a heat-shrink Teflon tubing mask, and the sample was scanned at 0.5 mV s^{-1} by using cyclic staircase voltammetry.

UV-visible spectroscopy was performed with a Hewlett Packard model 8543 diode-array spectrophotometer or a Varian CARY 5 spectrophotometer employing Wilmad no. 107-7 closed type 0.10 cm path length quartz cells. The solubility of Ti(II) in the melt was measured by using atomic absorption spectroscopy (Perkin-Elmer model 2380). Standard methods were employed.

The surface morphology and elemental analysis of alloy samples were investigated with a JEOL JSM-6100 scanning electron microscope (SEM) equipped with a Link energy dispersive X-ray spectrometer at the University of Mississippi SEM/EDX facility located in the Department of Mechanical Engineering or with a Hitachi S-4700 field-emission scanning electron microscope at the National Institute of Standards and Technology (NIST). The electrodeposits were also examined by X-ray diffraction (XRD) by using a Siemens D-500 diffractometer with Cu Kα radiation. The lattice parameters of the deposits were refined using the Cu substrate reflections as an internal standard. Transmission electron microscopy (TEM) was performed on selected deposits prepared for both plan view and cross-sectional analysis. The plan view films were detached from the planar Cu substrate and affixed to a Mo support ring. Cross sections of Al-Ti, deposited onto Cu wires, were formed by first overplating with Cu by using a cyanide Cu strike followed by bright Cu from a $CuSO_4$ solution.[27] Cross-sectional cuts, 0.75 mm thick, were then dimple polished down to 20 μm thickness. Plan view and cross sectional samples were subsequently milled with 4.5 kV Ar ions at 5 degrees incidence. Portions of the samples with electronic transparency were examined at 300 kV by using a JEOL 3010 TEM.

Results and Discussion

Dissolution of $TiCl_2$.—The dissolution of solid $TiCl_2$ was investigated as a method to supply Ti(II) in Lewis acidic $AlCl_3$-EtMeImCl melts for the electrodeposition of Al-Ti alloys. $TiCl_2$ dissolved slowly in these melts at 353.2 K. The solubility of $TiCl_2$ in the two melt compositions used for this investigation, 60.0-40.0 and 66.7-33.3 m/o $AlCl_3$-EtMeImCl, designated hereafter as the 60.0 and 66.7 m/o melts, respectively, was estimated by preparing saturated solutions of $TiCl_2$ in both melts at 353.2 K, dissolving a weighed portion of the supernatant liquid from these saturated solutions in distilled water, and determining the Ti(II) concentration with atomic absorption spectroscopy using standard methods. The results of these experiments are given in Table I. Because the solubility of $TiCl_2$ increases with increasing melt acidity, *i.e.*, with increasing $Al_2Cl_7^-$ concentration, the $TiCl_2$ dissolution reaction must be

$$2Al_2Cl_7^- + TiCl_2(s) \rightarrow [Ti(AlCl_4)_3]^- + AlCl_4^- \qquad [1]$$

However, as is shown later in this article, the Ti(II) species is likely to be polymeric or aggregated, especially when the Ti(II) is present at high concentrations. Thus, the simple six-coordinate structure for dissolved Ti(II) given in Eq. 1, which can be inferred from the EXAFS results of Dent *et al.*,[28] may be inadequate under these conditions. By contrast to $TiCl_2$, $TiCl_3$ was found to be insoluble in all compositions of the acidic $AlCl_3$-EtMeImCl melt.

Table I. Solubility of Ti(II) in acidic $AlCl_3$-EtMeImCl.

	$AlCl_3$-EtMeImCl		$AlCl_3$-NaCl
Temperature (K)	353		423
mol % $AlCl_3$	60.0	66.7	66.7
Solubility of Ti(II) (mmol L^{-1})	60 ± 1[a]	170 ± 2[b]	325[21]

Color of solutions: [a]dark green, [b]dark reddish-yellow.

A small amount of purple precipitate identical to solid $TiCl_3$ was present in the 60.0 m/o melt after the dissolution of $TiCl_2$, but was not obvious in the 66.7 m/o melt. The presence of $TiCl_3$ in solutions of $TiCl_2$ could arise through several different routes, including slow disproportionation of the dissolved Ti(II) as shown in Eq. 2

$$3[Ti(AlCl_4)_3]^- + 3AlCl_4^- \rightleftharpoons 2TiCl_3(s) + Ti + 6Al_2Cl_7^- \qquad [2]$$

or by oxidation of the Ti(II) through reaction with adventitious impurities in the melt or with oxygen in the glove box atmosphere. Sørlie and Øye[29] reported that Ti(II) tends to disproportionate in $AlCl_3$-KCl melts containing less than 60.0 m/o $AlCl_3$, where the $AlCl_4^-$ concentration is large, but is stable in strongly Lewis acidic melts.

In order to examine the stability of dissolved $TiCl_2$, the room-temperature UV-visible absorption spectra of Ti(II) in both 60.0 and 66.7 m/o $AlCl_3$-EtMeImCl were recorded as a function of concentration (Fig. 1). Dilute solutions of Ti(II) appeared pale green in the former melt and pale yellow-green in the latter melt. The principal absorption bands in these spectra are summarized in Table II. In the 60.0 m/o melt, Ti(II) exhibits bands at 344 and 444 nm, whereas the spectra of Ti(II) in 66.7 m/o melt show bands at 339 and 433 nm and a shoulder at 407 nm. In addition, the Ti(II) spectra in these two melts differed considerably at wavelengths greater than 500 nm. As shown in Table II, the absorption bands recorded in the acidic $AlCl_3$-EtMeImCl melt are in general shifted to higher energies compared to those observed in acidic $AlCl_3$-KCl melt.[29] A shift in the wavelengths of the absorption maxima was also observed with changes in the acidity of the $AlCl_3$-EtMeImCl melt. This shift is probably caused by changes in ligand field strength brought about by changes in the anionic speciation of the melt as the melt composition is changed.

Figure 2 shows the relationship between the Ti(II) concentration and the absorbance at 444 nm in the 60.0 m/o melt and 433 nm in the 66.7 m/o melt. These wavelengths correspond to the main bands in the spectra shown in Fig. 1. The plot constructed with absorbance data in the 66.7 m/o melt shows good adherence to Beer's law over the composition range that was examined. However, the absorbance of the 444 nm band in 60.0 m/o melt was generally smaller than that for the corresponding band in the 66.7 m/o melt, and most significantly, it did not obey Beer's law. There was no obvious evidence of $TiCl_3$ or titanium metal in the dilute solutions of Ti(II) in 60.0 m/o melt that were employed for this spectroscopic investigation. However, the spectra recorded in the 60.0 m/o melt exhibit a large wavelength-independent background absorbance (Fig. 1a-d). This phenomenon was most apparent at wavelengths above 500 nm and was absent from Ti(II) spectra recorded in the 66.7 m/o melt. This large background absorbance is attributed to light scattering by finely dispersed particulate matter in these solutions. We conclude from these observations and the nonlinearity of the Beer's law plot that Ti(II) slowly disproportionates in the 60.0 m/o melt. This implies that the potential of the Ti(II)/Ti couple is very close to that for the Ti(III)/Ti(II) couple. Thus, in view of the uncertainty about the

Downloaded on 2012-10-05 to IP 128.143.23.241 address. Redistribution subject to ECS license or copyright; see www.esltbd.org

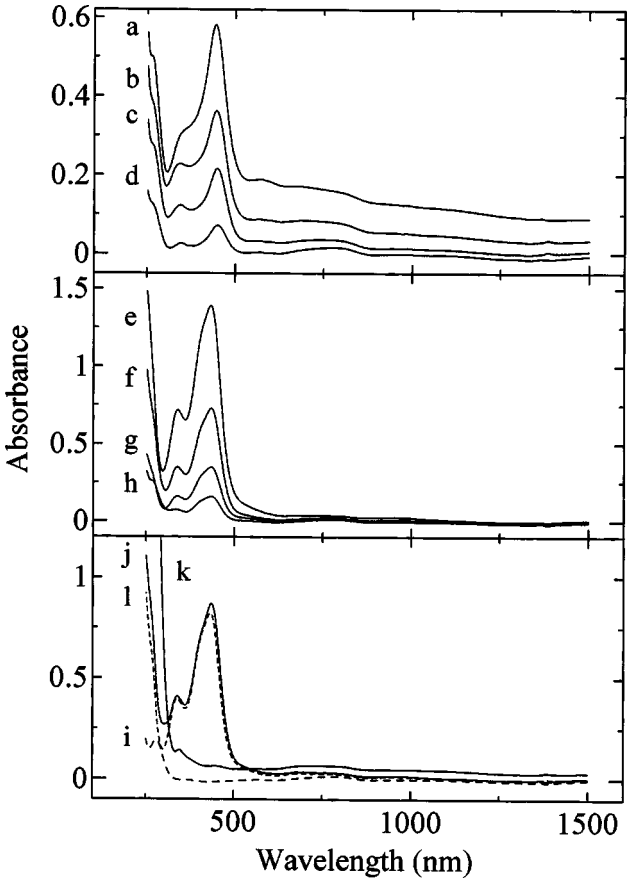

Figure 1. UV-vis absorption spectra of Ti(II) in the $AlCl_3$-EtMeImCl melt: (top) 60.0 m/o melt, Ti(II) concentrations: (a) 8.21, (b) 4.03, (c) 2.08, (d) 1.00 mmol L^{-1}; (middle) 66.7 m/o melt, Ti(II) concentrations: (e) 8.16, (f) 4.06, (g) 2.03, and (h) 1.01 mmol L^{-1}; (bottom) 66.7 m/o melt, (i) after stirring with sufficient $TiCl_3$ to prepare a 4.86 mmol L^{-1} solution, (j) after the addition of Al metal to the solution in (i) and stirring for several hours, (k) after the anodic oxidation of a Ti electrode at 0.60 V, and (l) after the addition of Al metal to the solution in (k) and stirring for several hours. All measurements were carried out in 0.10 cm path length quartz cells.

Ti(II) concentration and stability, we report herein only qualitative data for experiments carried out in the 60.0 m/o composition of the $AlCl_3$-EtMeImCl melt.

During previous investigations conducted in $AlCl_3$-NaCl-KCl, Ti(II) was introduced into the melt by the direct reduction of $TiCl_3$ or $TiCl_4$ with Al metal.[22] This method was investigated in 66.7 m/o

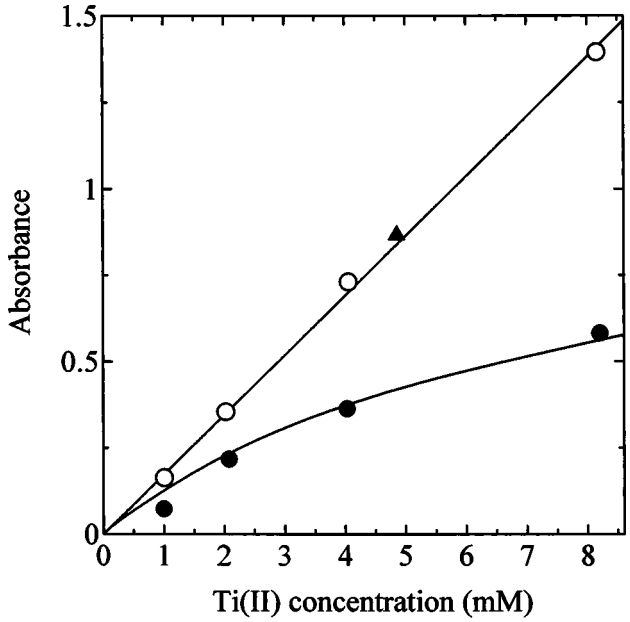

Figure 2. Beer's law plot for Ti(II) in the $AlCl_3$-EtMeImCl melt prepared from the data in Fig. 1: (●) 444 nm, 60.0 m/o melt, (○) 433 nm, 66.7 m/o melt, and (▲) the solution in Fig. 1j at 433 nm.

$AlCl_3$-EtMeImCl melt by reacting $TiCl_3$ with Ti or Al metal. No UV-vis spectrum was observed for Ti(III) in the supernatant liquid of melts containing solid $TiCl_3$, attesting further to its virtually complete insolubility in this melt. However, if sufficient powdered $TiCl_3$ was added to a known volume of melt to produce a 4.86 mmol L^{-1} solution and if this suspension of $TiCl_3$ was stirred with a small piece of aluminum metal at 353.2 K, then the solution became yellow-green and exhibited a spectrum identical to that for Ti(II) (Fig. 1j). Furthermore, the absorbance of the 433 nm band in this spectrum is in excellent agreement with the data for Ti(II) solutions shown in Fig. 2, indicating complete conversion of the $TiCl_3$ to Ti(II). This may be an important result because aluminum and titanium metal, as well as $TiCl_3$, are much less expensive than $TiCl_2$. Thus, the *in situ* reduction of $TiCl_3$ to soluble Ti(II) by titanium or aluminum metal may be a useful route for introducing Ti(II) into an organic chloroaluminate plating bath.

Electrochemical oxidation of Ti(II).—The electrochemistry of titanium has been investigated extensively in the 65.0 and 66.7 m/o $AlCl_3$-NaCl melts[18,30] and in the 66.7 m/o $AlCl_3$-EtMeImCl melt.[19] However, somewhat different approaches were used in these studies.

Table II. Summary of absorption spectral data.

Ionic species	Solvent	Temperature (K)	λ (nm)	Ref.
Ti(II)	$AlCl_3$-EtMeImCl (60.0-40.0 m/o)	~298	344[a],444	This work
	$AlCl_3$-EtMeImCl (66.7-33.3 m/o)	~298	340,407[a],433	This work
	$AlCl_3$-KCl (51.0-49.0 m/o)	562 ~ 654	357,453,702	29
	$AlCl_3$-KCl (66.7-33.3 m/o)	471 ~ 629	464,702	29
Ti(III)	$AlCl_3$-EtMeImCl (60.0-40.0 m/o)	~298	—	This work
	$AlCl_3$-EtMeImCl (66.7-33.3 m/o)	~298	—	This work
	$AlCl_3$-KCl (51.0-49.0 m/o)	746 ~ 894	—	29
	$AlCl_3$-KCl (66.7-33.3 m/o)	479 ~ 553	465,690	29
Ti(IV)	$AlCl_3$-EtMeImCl (60.0-40.0 m/o)	~298	288	This work
	$AlCl_3$-EtMeImCl (66.7-33.3 m/o)	~298	287	This work
	$AlCl_3$-EtMeImCl (60.0-40.0 m/o)	~298	290	19

[a] Shoulder.

Downloaded on 2012-10-05 to IP 128.143.23.241 address. Redistribution subject to ECS license or copyright; see www.esltbd.org

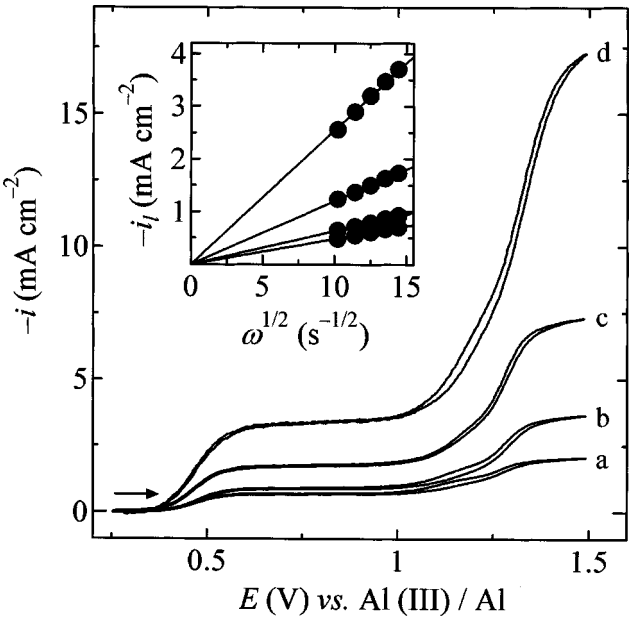

Figure 3. Voltammograms recorded at a Pt-RDE at 353.2 K in the 66.7 m/o $AlCl_3$-EtMeImCl melt at 2000 rpm. The Ti(II) concentrations were (a) 12.6, (b) 25.2, (c) 50.3, and (d) 170 mmol L^{-1}. The sweep rates were 0.01 V s^{-1}. Inset: Levich plot constructed from limiting current data at 0.75 V.

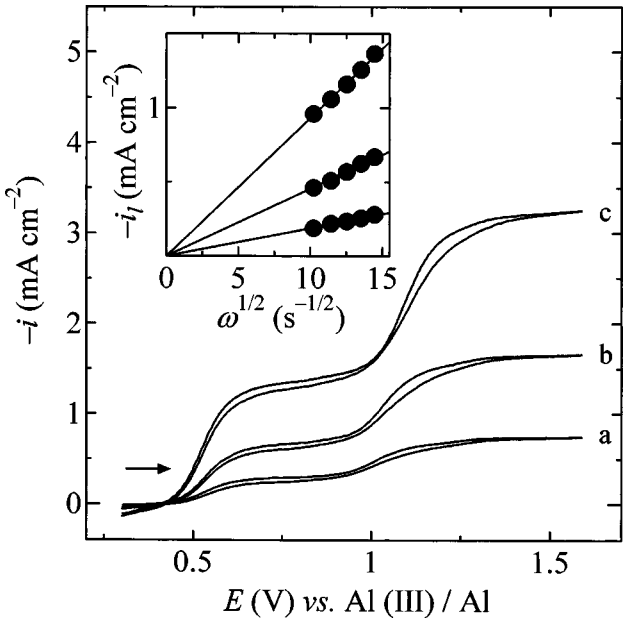

Figure 4. Voltammograms recorded at a Pt-RDE at 353.2 K in the 60.0 m/o $AlCl_3$-EtMeImCl melt at 2000 rpm. The Ti(II) concentrations were (a) 8.30, (b) 16.7, and (c) 52.5 mmol L^{-1}. The sweep rates were 0.01 V s^{-1}. Inset: Levich plot constructed from limiting current data at 0.75 V.

For example, experiments in former ionic solvent were carried out with dissolved $TiCl_2$ or electrogenerated Ti(II) as the starting material at elevated temperatures (>423 K), whereas experiments involving the latter melt were carried out at ambient temperature with $TiCl_4$ as the titanium solute. Regardless of the oxidation state of the starting species, all of these investigations revealed that the electrochemistry of titanium is dominated by the two one-electron, quasi-reversible electrode reactions shown below

$$\mathrm{Ti(IV)} + \mathrm{e}^- \rightleftharpoons \mathrm{Ti(III)} \quad [3]$$

$$\mathrm{Ti(III)} + \mathrm{e}^- \rightleftharpoons \mathrm{Ti(II)} \quad [4]$$

Furthermore, at slow voltammetric scan rates or long times, both the oxidation of Ti(II) and the reduction of Ti(IV) are complicated by the insolubility of Ti(III), which precipitates as red-violet or purple $TiCl_3$.

The electrochemical behavior of Ti(II) varied considerably with the melt composition. Figures 3 and 4 show Pt-RDE voltammograms of Ti(II) dissolved in the 66.7 and 60.0 m/o $AlCl_3$-EtMeImCl melts, respectively, at 353.2 K. These voltammograms were recorded at different Ti(II) concentrations. The voltammograms in these figures are very similar in appearance to the sampled current voltammogram for Ti(II) reported in the classic article by Fung and Mamantov[18] in that they exhibit two waves that can be ascribed to the reactions given in Eq. 3 and 4. The first waves in Fig. 3 and 4, which correspond to the reverse of Eq. 4, exhibit well-defined limiting currents in the 0.6 to 1.0 V potential range at all of the Ti(II) concentrations that were studied. Levich plots, *i.e.*, plots of the limiting current or current density *vs.* the square root of the electrode rotation rate, for this wave were linear and passed through the origins of the plots (see insets of Fig. 3 and 4). However, the limiting current for the first wave at a fixed rotation rate did not scale linearly with the formal Ti(II) concentration as predicted by the Levich equation. This deviation was more obvious in the more acidic 66.7 m/o melt than in the 60.0 m/o melt. A similar deviation between the cyclic voltammetric peak current for the oxidation of Ti(II) at a platinum electrode and the formal Ti(II) concentration was also noted during experiments carried out in the Lewis acidic $AlCl_3$-NaCl melt.[18,21,30] This unusual behavior was attributed to the formation of a polymeric or aggregated species, $\{\mathrm{Ti(II)}\}_n$,[31] in the melt as the Ti(II) concentration was increased, which leads to a diffusing entity with a larger solvodynamic radius and correspondingly smaller diffusion coefficient. This electroinactive polymeric species was postulated to be in rapid equilibrium with the electroactive monomeric Ti(II) species. The data presented above indicate that the formation of Ti(II) polymers must also take place in the Lewis acidic $AlCl_3$-EtMeImCl melt. Furthermore, the Ti(II) aggregation process seems to be dependent on the melt acidity, becoming more extensive as the melt is made more acidic.

Diffusion coefficients for Ti(II), $D_{\mathrm{Ti(II)}}$, in the 66.7 m/o $AlCl_3$-EtMeImCl melt at 353.2 K were estimated from the slopes of Levich plots at each of the formal Ti(II) concentrations. [Uncertainty about the Ti(II) concentration precluded such calculations for solutions of Ti(II) in the 60.0 m/o melt]. The viscosity data reported by Fannin *et al.*[32] were used for these calculations. The experimental limiting current densities, i_1, and the estimated values of $D_{\mathrm{Ti(II)}}$ are given in Table III along with the Stokes-Einstein products, $D_{\mathrm{Ti(II)}}\eta/T$, where η and T are the absolute viscosity of the melt and the absolute temperature, respectively. As shown in Table III, the value of $D_{\mathrm{Ti(II)}}$ decreases as the formal concentration of Ti(II) increases in concordance with previous findings in acidic $AlCl_3$-NaCl melt.[18,21,30]

The second oxidation waves shown in Fig. 3 and 4 exhibit a distorted appearance. In some cases, the limiting currents for these waves are larger than the limiting currents for the first oxidation

Table III. Summary of electrochemical data for Ti(II) at 353.2 K

Mol % $AlCl_3$	Ti(II) formal concentration (mmol L^{-1})	i_1 (mA cm^{-2})	10^8 $D_{\mathrm{Ti(II)}}$ (cm^2 s^{-1})	10^{12} $\eta D_{\mathrm{Ti(II)}}/T$ (g cm s^{-2} K^{-1})
66.7	12.6	0.72	22.2	30.5
	25.2	0.94	11.8	16.2
	50.3	1.78	10.9	15.0
	95.4	3.21	9.97	13.7
	170	3.40	5.47	7.51

Downloaded on 2012-10-05 to IP 128.143.23.241 address. Redistribution subject to ECS license or copyright; see www.esltbd.org

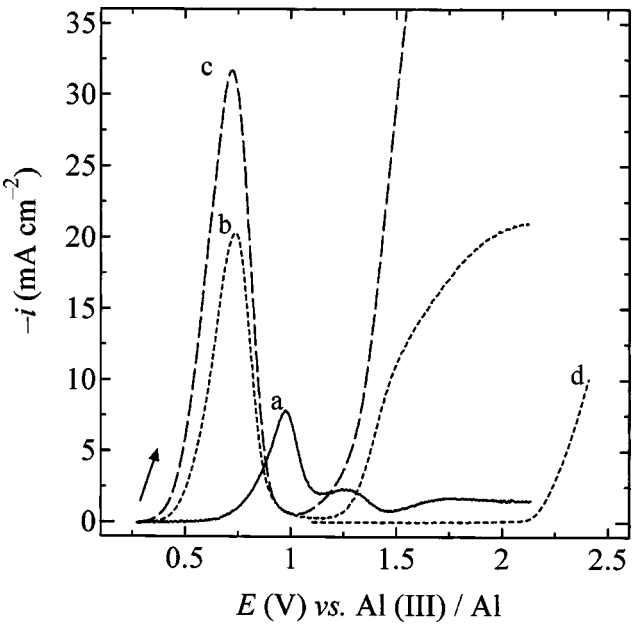

Figure 5. Linear sweep voltammograms recorded as a function of temperature in the 66.7 m/o $AlCl_3$-EtMeImCl melt: (a) Ti disk electrode, room temperature; (b) Ti disk electrode, 353.2 K; (c) Ti disk electrode, 373.2 K; and (d) Pt disk electrode at room temperature. The potential sweep rates were 0.01 V s^{-1}.

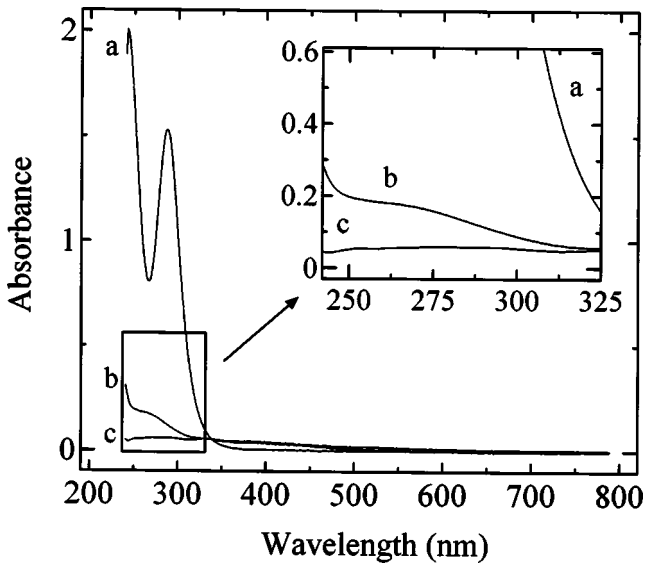

Figure 6. UV-vis absorption spectra recorded in 60.0 m/o $AlCl_3$-EtMeImCl melt: (a) 1.57 mmol L^{-1} $TiCl_4$ at room temperature, (b) after anodic polarization of a Ti electrode in neat melt at 0.05 mA cm^{-2} at 353.2 K, and (c) after the solution in (a) was heated to 353.2 K for 12 h.

waves, suggesting that the oxidation of Ti(III) to Ti(IV) is a complex process. Additional experiments beyond the scope of the present investigation are needed in order to deduce the mechanism leading to these results.

Anodic dissolution of titanium metal.—Anodic linear sweep voltammograms that were recorded at a stationary titanium disk electrode in the 66.7 m/o melt as a function of temperature are shown in Fig. 5. At room temperature, the titanium electrode must be scanned to approximately 0.60 V before dissolution commences. As the temperature of the melt was raised to 353.2 K and higher, the potential for the onset of titanium dissolution decreased. At all of the temperatures that were investigated, oxidation of the titanium metal electrode produced only a single well-defined wave and proceeded until the electrode was covered with a passive film of $TiCl_3$(s), which blocked the electrode. At elevated temperatures, *e.g.*, 353.2 and 373.2 K, this film breaks down when the potential is scanned above about 1.0 V as signaled by a sharp rise in the anodic current and the production of Ti(IV) in agreement with the voltammograms in Fig. 3. However, if the potential of the titanium electrode is scanned above 1.0 V at room temperature, a small current flows, but there is no appreciable breakdown of the $TiCl_3$ passive film that would signal the generation of Ti(IV). Because Ti(II) is a stable oxidation state of titanium in the 66.7 m/o melt (vide supra), it is unlikely that the first oxidation wave in the voltammograms shown in Fig. 5 arises from the direct, single-step, three-electron oxidation of Ti(0) to $TiCl_3$. Instead, the first wave probably reflects the successive reactions shown below

$$Ti(0) + 3AlCl_4^- \rightleftharpoons [Ti(AlCl_4)_3]^- + 2e^- \quad [5]$$

$$[Ti(AlCl_4)_3]^- + 3AlCl_4^- \rightleftharpoons TiCl_3(s) + 3Al_2Cl_7^- + e^- \quad [6]$$

Because only a single oxidation wave is observed in the 0.5 to 1.0 V potential region, the potentials for these reactions must be closely spaced, and/or a large overpotential must be required to initiate the reaction in Eq. 5, which shifts the potential of this reaction to a potential that overlaps with the reaction in Eq. 6. The presence of a large oxidation overpotential is also consistent with the observed temperature dependence of the potential at which the onset of titanium oxidation is observed.

To further investigate the oxidation of titanium metal in the $AlCl_3$-EtMeImCl melt, the anodic polarization of a titanium electrode with a large surface area was carried out in the 60.0 and 66.7 m/o melts at 353.2 K by using galvanostatic and potentiostatic methods. During galvanostatic electrolysis at low current density (~0.05 mA cm^{-2}), the potential was approximately 0.60 V at the outset of the experiment, but quickly increased to 1.15 V. At the conclusion of this electrolysis experiment, the color of the melt was pale yellow and no $TiCl_3$ precipitate was present in the cell. From the relationship between the charge passed and weight loss of the titanium wire, the number of electrons involved in the reaction was calculated from Faraday's law to be approximately 4, suggesting that the galvanostatic oxidation of titanium at the modest current density of this experiment produces $TiCl_4$. The direct oxidation of Ti metal to Ti(IV) at large positive potentials without the formation of a passive film of solid $TiCl_3$ was noted by Stafford and Moffat[30] during previous work carried out in 66.7 m/o $AlCl_3$-NaCl.

Figure 6 compares the UV-visible spectrum of the 60.0 m/o melt containing 1.57 mmol L^{-1} $TiCl_4$ and a spectrum of the solution resulting from the galvanostatic polarization of Ti metal as described above. the spectrum of the $TiCl_4$ solution is in excellent agreement with that reported by Carlin *et al.*[19] and consists primarily of a single band centered at 288 nm (Table II). However, only a weak band was found at this wavelength in the melt at the conclusion of the experiment. When a melt solution containing dissolved $TiCl_4$ was heated to 353.2 K with stirring, the spectrum of Ti(IV) gradually disappeared as the $TiCl_4$ vaporized from the melt. A cyclic voltammogram acquired at the conclusion of the electrolysis experiment gave a similar result. Taken together, the spectroscopic and voltammetric results indicate that the Ti(IV) produced by the anodic oxidation of titanium at 353.2 K evaporates from the melt during and after the electrolysis as $TiCl_4$(g). These results suggest that galvanostatic electrolysis is not a good method for introducing Ti(II) because of the difficulty of controlling the oxidation potential.

To circumvent the direct oxidation of Ti metal to Ti(IV), potentiostatic electrolysis was carried out in the 66.7 and 60.0 m/o melts at an applied potential of 0.60 V. However, the electrolysis current

Downloaded on 2012-10-05 to IP 128.143.23.241 address. Redistribution subject to ECS license or copyright; see www.esltbd.org

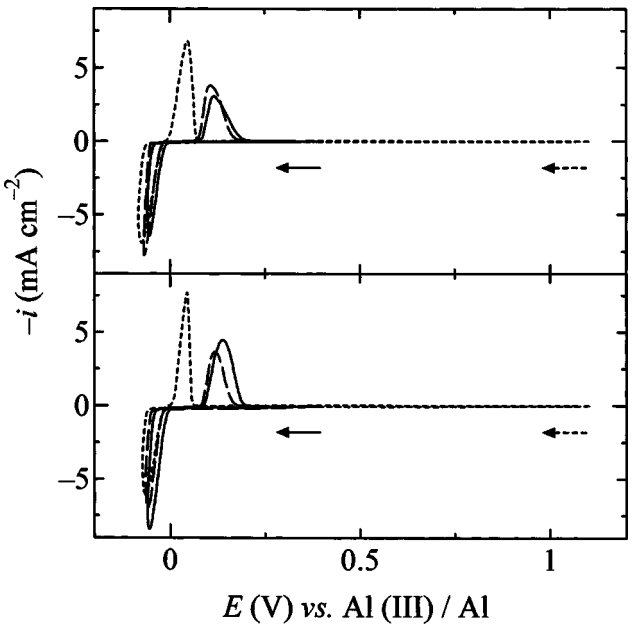

Figure 7. Cyclic voltammograms recorded at a (top) stationary and (bottom) rotating Pt-RDE (2000 rpm) in the 60.0 m/o $AlCl_3$-EtMeImCl melt at 353.2 K: (– – –) neat melt, (— — —) 40.4 mmol L^{-1} Ti(II), and (——) 59.5 mmol L^{-1} Ti(II). The potential sweep rates were 0.01 V s^{-1}.

diminished to nearly zero, and the electrode became coated with a reddish-purple film of $TiCl_3$ shortly after the electrolysis commenced. An absorption spectrum of this solution showed that no Ti(II) was obtained (Fig. 1k). Vigorous stirring did not lead to a different result, but merely dislodged the solid $TiCl_3$ from the electrode as it was formed. However, if this solution was stirred with Ti or Al metal for several hours at 353.2 K, the $TiCl_3$ precipitate disappeared, and the absorption spectrum of the solution became identical to that for Ti(II) (Fig. 1).

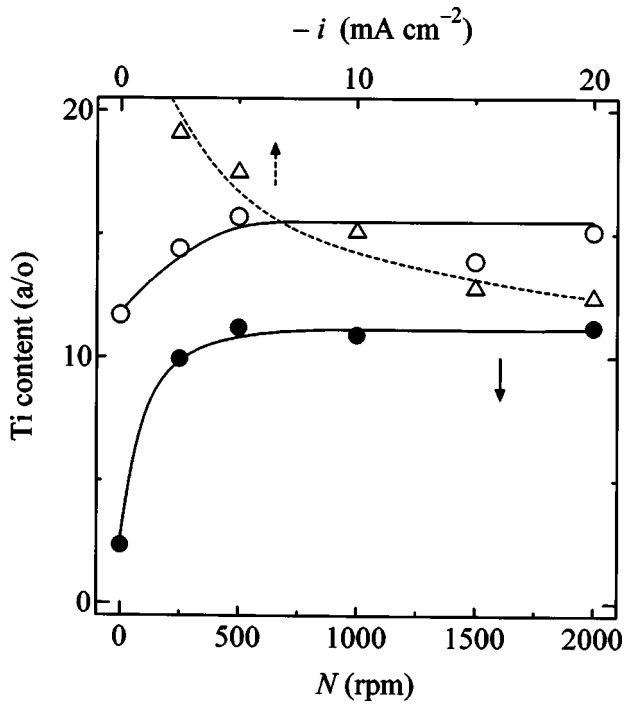

Figure 8. Relationship between the electrode rotation rate, the current density, and the titanium content of bulk Al-Ti alloys deposited from Ti(II)-saturated $AlCl_3$-EtMeImCl melts at 353.2 K: (●) 60.0 m/o melt, −10 mA cm^{-2}, (○) 66.7 m/o melt, −10 mA cm^{-2}, and (△) 66.7 m/o melt as a function of the current density at a rotation rate of 2000 rpm.

Table IV. Al-Ti alloy composition as a function of the electrode rotation rate.

	Mol % $AlCl_3$	Rotation rate (rpm)					
		0	250	500	1000	1500	2000
Titanium	60.0	2.4	9.9	11.2	10.9	—	11.2
content (a/o)	66.7	11.7	14.4	15.7	—	13.9	15.1

Electrodeposition of Al-Ti alloys.—Figure 7 shows cyclic voltammograms for stationary and rotating Pt disk electrodes in the 60.0 m/o melt with and without added Ti(II). It was demonstrated during a previous investigation in acidic $AlCl_3$-NaCl melt that the potential of the Al stripping wave shifts positively after the addition of Ti(II).[21] This behavior occurs because Ti metal co-deposits with Al metal to form Al-Ti alloy, which is more difficult to oxidize than pure Al. Similar behavior was observed in $AlCl_3$-EtMelmCl containing Ti(II). Furthermore, the magnitude of this shift increased with increasing Ti(II) concentration. Virtually identical results were observed in the 66.7 m/o $AlCl_3$-EtMeImCl melt. However, the addition of Ti(II) to acidic $AlCl_3$-EtMeImCl melt did not increase the overpotential for Al deposition as found for Ti(II) solutions in $AlCl_3$-NaCl. In fact, a small positive shift was evident.

In order to investigate the formation of bulk Al-Ti alloys, electrodeposition was performed by using dc galvanostatic methods at a current density of −10 mA cm^{-2} in a Ti(II)-saturated melt. The substrate for these experiments was a copper rotating disk electrode (Cu-RDE). As shown in Fig. 8 and Table IV, the Ti metal content of the Al-Ti alloys depends on the electrode rotation rate at small rotation rates, but becomes independent of a rotation rate above 500 rpm. Therefore, all deposition experiments were conducted at rotation rates exceeding 500 rpm.

In the 66.7 m/o $AlCl_3$-NaCl melt at 423.2 K at Ti(II) concentrations greater than 150 mmol L^{-1}, the Ti metal content of the Al-Ti alloy became virtually independent of the current density, and $TiAl_3$ with an ordered $L1_2$ crystal structure was the predominant alloy produced.[21,30] However, different results were obtained in the 66.7 m/o $AlCl_3$-EtMeImCl melt at 353.2 K. Although solutions containing more than 150 mmol L^{-1} Ti(II) can be prepared in this melt without difficulty (Table I), the Ti metal content of bulk Al-Ti alloys prepared in these solutions was found to increase as the applied current density is decreased (Table V and Fig. 8). This result is to be expected if the reduction potential of the Ti(II)/Ti couple is positive of that for Al(III)/Al because at low reduction current densities and correspondingly less negative potentials, the partial current density for the electrodeposition of Ti metal would be a larger fraction of the total current density. At larger reduction current densities or more negative potentials, the partial current for Ti metal probably reaches its mass-transport-limited value, whereas the partial current density for the deposition of Al metal continues to increase relative to the Ti metal deposition current density, becoming a larger fraction of the total current and resulting in alloy deposits with a smaller fraction of Ti metal. The results of this investigation indicate that the titanium content of Al-Ti alloys electrodeposited from the $AlCl_3$-EtMeImCl

Table V. Electrodeposited Al-Ti alloys.

	mol % $AlCl_3$	Electrodeposition current density (mA cm^{-2})				
		−2.5	−5.0	−10.0	−15.0	−20.0
Titanium	66.7	19.1	17.5	15.1	12.8	12.4
content (a/o)						

Downloaded on 2012-10-05 to IP 128.143.23.241 address. Redistribution subject to ECS license or copyright; see www.esltbd.org

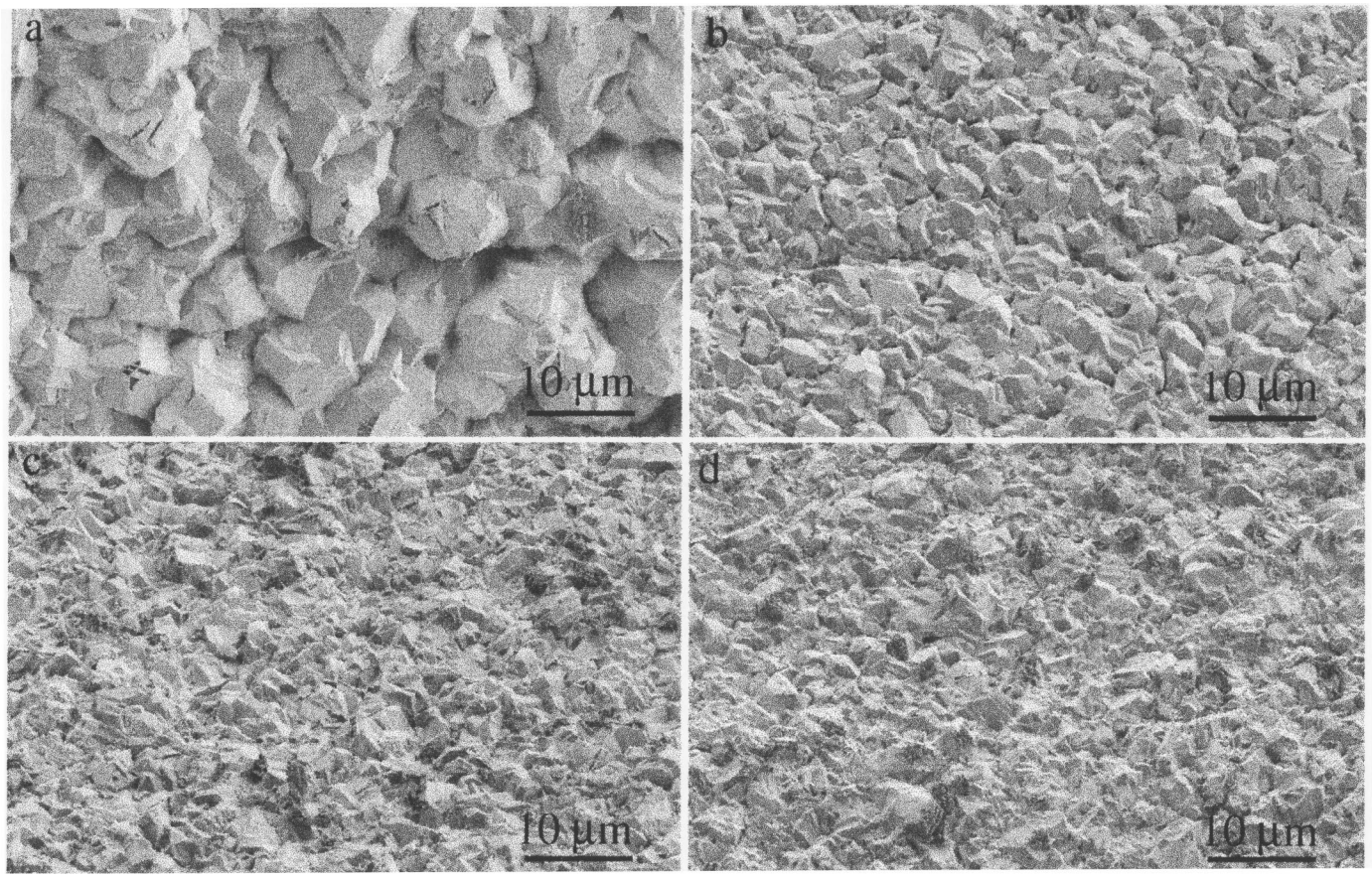

Figure 9. Field-emission scanning electron micrographs of Al-Ti alloys electrodeposited at 353.2 K from 66.7 m/o $AlCl_3$-EtMeImCl melt containing 170 mmol L^{-1} Ti(II). The current density and alloy compositions were (a) -20.0 mA cm^{-2}, 7.0 a/o Ti; (b) -5.00 mA cm^{-2}, 11.4 a/o Ti; (c) -1.00 mA cm^{-2}, 15.6 a/o; and (d) -0.50 mA cm^{-2}, 18.4 a/o Ti.

melt is limited by the solubility of $TiCl_2$ and the minimum practical current density that can be used for the timely preparation of such deposits.

Characterization of Al-Ti electrodeposits.—The morphologies of four electrodeposits are shown in Fig. 9. In this figure, the current density is decreased from -20 mA cm^{-2} in Fig. 9a to -0.50 mA cm^{-2} in Fig. 9d. This corresponds to an increase in the Ti metal content from 7.0 to 18.4 a/o. In all cases, the deposits were nodular, compact, and dense. Many of the nodules showed crystallographic faceting, although no symmetry characteristic of a particular growth direction was observed. It is clear that the nodule size decreases with decreasing current density and increasing titanium content. Typically one would expect an increase in grain size as the deposition current density or overpotential is decreased. However, in this case, the grain refinement is driven by the incorporation of Ti metal into the alloy rather than the deposition overpotential. This nicely demonstrates the impact that impurities and alloying additions have on deposit morphology. A high magnification view of the 18.4 a/o Al-Ti deposit (Fig. 9d) is shown in Fig. 10. The step faceting is clearly seen in each nodule, confirming that the nodules are single crystals. It also suggests that although the macrodeposit grows by three-dimensional nucleation and growth, each nodule grows primarily by two-dimensional, layered growth.

Electrodeposits containing 7.0 to 18.4 a/o Ti metal were examined by X-ray diffraction (XRD) methods. All of the diffraction patterns were indexed to a disordered face-centered cubic (fcc) structure and were very similar to that of pure aluminum. Two distinct changes in the diffraction patterns with increased Ti metal content of the alloy were observed. The first was a 0.33% decrease in the aluminum lattice parameter over this range of composition. This is to be expected as the smaller Ti atoms substitute for Al in the fcc lattice. The second change was significant broadening of the X-ray reflections with increasing Ti metal content, suggesting a decrease in the deposit grain size. This latter result supports the SEM analysis that showed a decrease in grain size with an increase in the Ti metal content (Fig. 9).

The chemically disordered fcc structure obtained in this study from the room temperature melt is a significant departure from the ordered $L1_2$ crystal structure deposited from $AlCl_3$-NaCl at 423.2 K.[20,33] Figure 11 shows the XRD patterns of Al-Ti films electrodeposited at 353.2 K from $AlCl_3$-EtMeImCl and at 423.2 K from $AlCl_3$-NaCl. For comparison, a calculated diffraction pattern for fully ordered ($L1_2$) Al_3Ti is shown.[34] The diffraction pattern of the 423.2 K deposit clearly shows the 100 and 110 superlattice reflections of the ordered $L1_2$ structure. High-resolution TEM indicates that the $L1_2$ domains are on the order of 5-10 nm in size.[33] This explains the significant line broadening seen in the superlattice reflections for the higher temperature electrodeposit (Fig. 11b). The superlattice reflections are clearly absent from the diffraction pattern of the alloy deposited at 353.2 K. In addition, the 111 fundamental reflection is shifted to lower values of 2θ, reflecting the larger lattice parameter as a result of the substoichiometric Ti metal content. Extensive broadening of the superlattice reflections might make them difficult to detect by XRD. A report in the literature describing a glancing angle X-ray examination of Al-Ti alloys electrodeposited from eutectic $AlCl_3$-NaCl-KCl containing Ti(III) also shows the fundamental reflections for fcc Al for compositions containing up to 27.5 a/o Ti metal. However, the authors were unable to confirm the

Downloaded on 2012-10-05 to IP 128.143.23.241 address. Redistribution subject to ECS license or copyright; see www.esltbd.org

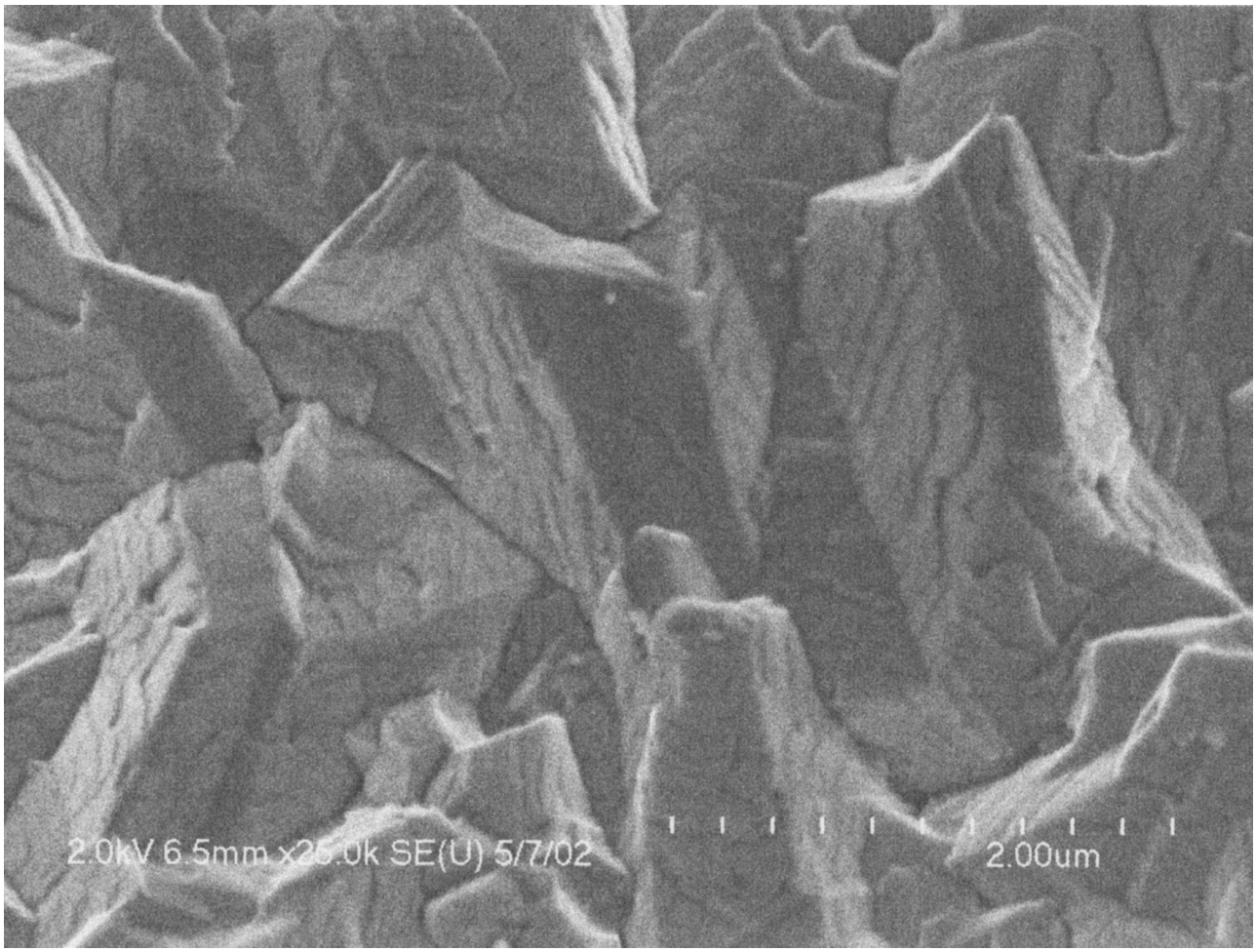

Figure 10. Field-emission scanning electron micrograph with increased magnification of the alloy sample shown in Fig. 9.

$L1_2$ structure due to the lack of superlattice reflections in the XRD pattern.[22]

In order to confirm the chemical disorder in the Al-Ti deposited from $AlCl_3$-EtMeImCl melt, electron diffraction analysis of selected electrodeposits in both plan view and cross section was performed (Fig. 12). A typical diffraction pattern taken on the [001] zone axis from a deposit containing 18.4 a/o Ti metal is shown in Fig. 12a. The pattern is consistent with single-phase fcc Al-Ti having a lattice parameter close to 0.405 nm. No superlattice reflections were found in any of the diffraction patterns indicating that the detected phase has a random ordering of Al and Ti atoms. For comparison, the diffraction patterns from films containing 16.0 a/o Ti and 24.0 a/o Ti, both deposited from $AlCl_3$-NaCl at 423.2 K are shown in Fig. 12b and c, respectively.[20] The 100 and 110 superlattice reflections are clearly visible, and their intensities grow progressively relative to the fundamental 200 spots as the titanium concentration is increased. The presence of superlattice reflections indicates that the crystal structure of the 423.2 K deposits is not disordered fcc because the 100 and 110 reflections are forbidden for the fcc lattice. It is also clear from Fig. 12 that the chemical disorder of the room temperature melt deposit is not simply due to the low Ti content. The 16.0 a/o Ti alloy deposited from $AlCl_3$-NaCl clearly shows the superlattice reflections indicative of $L1_2$ ordering, Fig. 12b, even though the composition is less than stoichiometric Al_3Ti.

The electrodeposited Al_3Ti described above displays crystallographic features of distinctly different length scales. The grain size of all electrodeposits examined is on the order of 0.5 to 5 μm. Deposits formed at 353.2 K are chemically disordered whereas those formed at 423.2 K have $L1_2$ domains measuring 5-10 nm in size. Previous work suggests that these domains appear to have grown through a first-order nucleation and growth process, independent of the electrocrystallization process.[33] This type of domain structure is quite common in rapidly solidified alloys wherein the disordered phase produced by the solidification process transforms to the equilibrium ordered phase quite rapidly during solid-state cooling to room temperature.[35] Although this often occurs at temperatures that do not allow for significant bulk diffusion, the activation barrier to the nucleation of ordered domains is rather small because both the nucleus and matrix have essentially the same crystal structure and composition.[36] Consequently, nucleation tends to be homogeneous and independent of lattice defects. These results strongly suggest that the Al-Ti alloy deposits in the disordered state and that ordering occurs in the solid state, subsequent to the charge-transfer step and adatom incorporation into the lattice. The degree of chemical order-disorder is directly linked to the deposition temperature.

Pitting potential measurements.—Potentiodynamic anodic polarization curves recorded in deaerated aqueous NaCl for Al-Ti alloys electrodeposited on copper wire electrodes are shown in Fig. 13. As noted for Al-Mn alloys examined under similar conditions,[37] Al-Ti alloys display a stable passive region characterized by a very small

Downloaded on 2012-10-05 to IP 128.143.23.241 address. Redistribution subject to ECS license or copyright; see www.esltbd.org

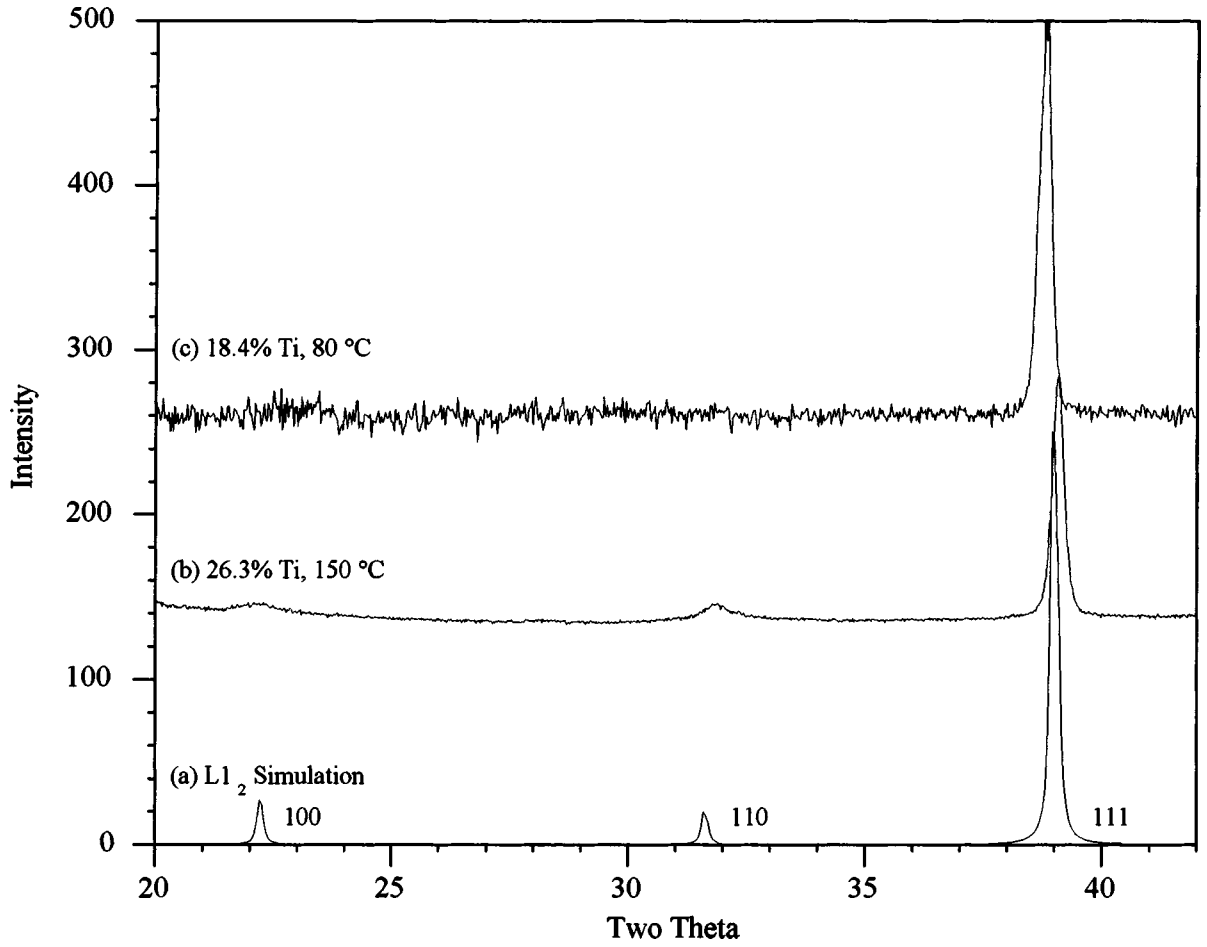

Figure 11. (a) Calculated XRD pattern for fully ordered ($L1_2$) Al_3Ti[34] and experimental XRD patterns (Cu Kα) from as-deposited Al-Ti alloys containing (b) 26.3 a/o Ti that was deposited from 66.7 m/o $AlCl_3$-NaCl at 423.2 K, and (c) 18.4 a/o Ti that was deposited from 66.7 m/o $AlCl_3$-EtMeImCl at 353.2 K.

potential-independent current followed by a sudden rise in current at the pitting potential. The variation of the pitting potential with alloy composition is shown in Fig. 14. The addition of ~8 a/o Ti metal increases the pitting potential of the alloy by about 0.30 V; however, alloys containing ~15 a/o Ti metal show only a 0.45 V increase in pitting potential relative to pure Al. Thus, the greatest benefit is realized by the addition of a relatively modest amount of Ti metal. This same result was noted for electrodeposited Al-Mn alloys, except that the formation of a two-phase fcc + glass structure for alloys containing more than 5 a/o Mn led to a decrease in the pitting

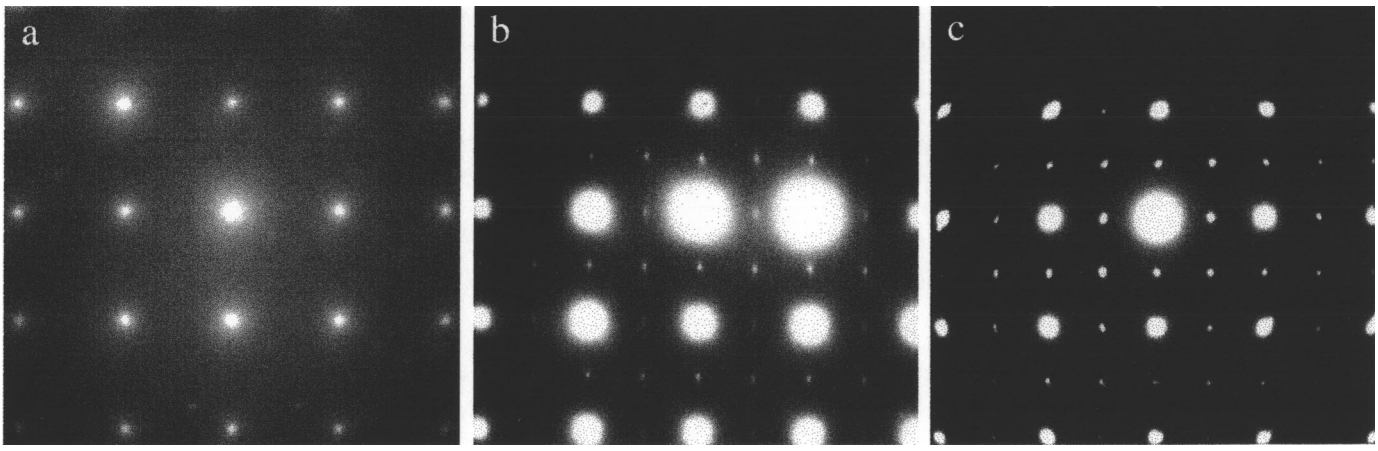

Figure 12. Selected area diffraction patterns of Al-Ti alloys taken on the [001] zone axis from as-deposited Al-Ti alloys containing (a) 18.4 a/o Ti deposited from 66.7 m/o $AlCl_3$-EtMeImCl at 353.2 K, (b) 16.0 a/o Ti deposited from 66.7 m/o $AlCl_3$-NaCl at 423.2 K, and (c) 24.0 a/o Ti deposited from 66.7 m/o $AlCl_3$-NaCl at 423.2 K.[20]

Downloaded on 2012-10-05 to IP 128.143.23.241 address. Redistribution subject to ECS license or copyright; see www.esltbd.org

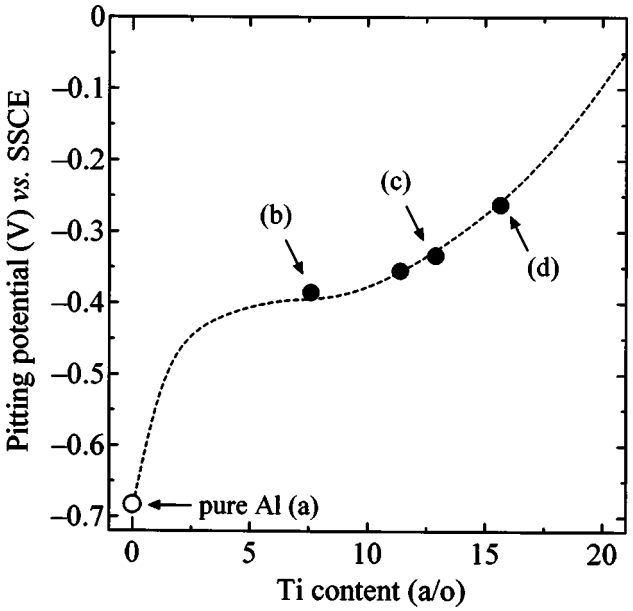

Figure 13. Potentiodynamic polarization curves for Al and Al-Ti alloys in deaerated 0.1 M aqueous NaCl: (a) Al (99.999%), (b) $Al_{92.4}Ti_{7.6}$, (c) $Al_{88.6}Ti_{11.4}$, and (d) $Al_{84.3}Ti_{15.7}$. The potential sweep rates were 0.5 mV s^{-1}.

potential.[37] The increase in the pitting potential observed for electrodeposited Al-Ti alloys is comparable to that found for Al-Ti alloys prepared by sputter deposition.[13]

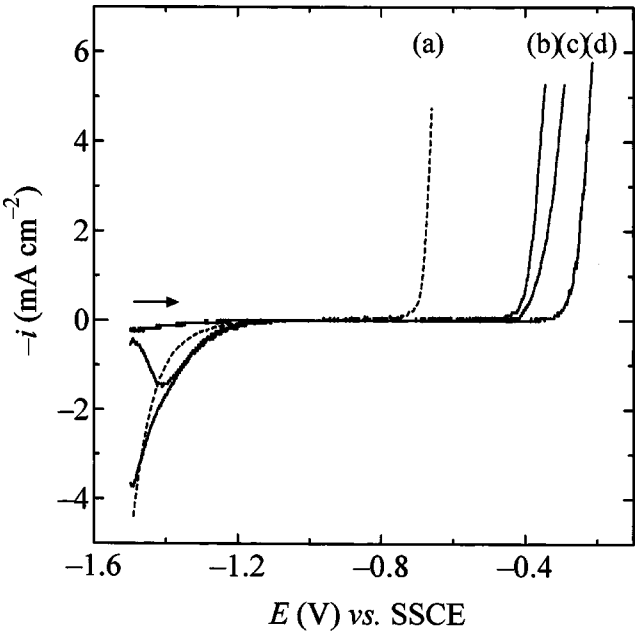

Figure 14. Pitting potentials as a function of the Ti content of the Al-Ti alloys in Fig. 13: (a) Al (99.999%), (b) $Al_{92.4}Ti_{7.6}$, (c) $Al_{88.6}Ti_{11.4}$, and (d) $Al_{84.3}Ti_{15.7}$.

Acknowledgments

This research was supported by the Air Force Office of Scientific Research, Grant no. F49620-00-1-0123.

The University of Mississippi assisted in meeting the publication costs of this article.

References

1. G. S. Frankel, R. C. Newman, C. V. Jahnes, and M. A. Russak, *J. Electrochem. Soc.*, **140**, 2192 (1993).
2. J. R. Davis, *Corrosion of Aluminum and Aluminum Alloys*, ASM International, Materials Park, OH (1999).
3. W. C. Moshier, G. D. Davis, and G. O. Cote, *J. Electrochem. Soc.*, **136**, 356 (1989).
4. P. Furrer and H. Warlimont, *Mater. Sci. Eng.*, **28**, 127 (1977).
5. M. Fass, D. Itzhak, D. Eliezer, and F. H. Froes, *J. Mater. Sci.*, **6**, 1227 (1987).
6. A. H. Al-Saffar, V. Ashworth, A. K. O. Bairamov, D. J. Chivers, W. A. Grant, and R. P. M. Procter, *Corros. Sci.*, **20**, 127 (1980).
7. M. V. Zeller and J. A. Kargol, *Appl. Surf. Sci.*, **18**, 63 (1984).
8. P. M. Natishan, E. McCafferty, and G. K. Hubler, *J. Electrochem. Soc.*, **135**, 321 (1988).
9. A. S. Edelstein, R. K. Everett, J. H. Perepezko, and M. H. da Silva Bassani, *J. Mater. Res.*, **12**, 385 (1997).
10. K. Honda, A. Hirose, and K. F. Kobayashi, *Mater. Sci. Eng., A*, **222**, 212 (1996).
11. H. C. Chen and E. Pfender, *Thin Solid Films*, **280**, 188 (1996).
12. W. C. Moshier, G. D. Davis, J. S. Ahearn, and H. F. Hough, *J. Electrochem. Soc.*, **134**, 2677 (1987).
13. G. S. Frankel, M. A. Russak, C. V. Jahnes, M. Mirzamaani, and V. A. Brusic, *J. Electrochem. Soc.*, **136**, 1243 (1989).
14. G. D. Davis, W. C. Moshier, T. L. Fritz, and G. O. Cote, *J. Electrochem. Soc.*, **137**, 422 (1990).
15. B. A. Shaw, G. D. Davis, T. L. Fritz, B. J. Rees, and W. C. Moshier, *J. Electrochem. Soc.*, **138**, 3288 (1991).
16. R. Banerjee, R. Ahuja, and H. L. Fraser, *Phys. Rev. Lett.*, **76**, 3778 (1996).
17. M. Fahoume, M. El Khamlichi, C. Baltzinger, and C. Burggraf, *Mater. Res. (Zug. Switz)*, **1-2**, 391 (1994).
18. K. W. Fung and G. Mamantov, *J. Electroanal. Chem.*, **35**, 27 (1972).
19. R. T. Carlin, R. A. Osteryoung, J. S. Wilkes, and J. Rovang, *Inorg. Chem.*, **29**, 3003 (1990).
20. G. M. Janowski and G. R. Stafford, *Metall. Mater. Trans. A*, **23**, 2715 (1992).
21. G. R. Stafford, *J. Electrochem. Soc.*, **141**, 245 (1994).
22. J. Uchida, H. Seto, and A. Shibuya, *J. Surf. Finishing Soc. of Jpn, (Hyomen Gijutsu)*, **46**, 1167 (1995).
23. H.-Y. Hsu, D.-L. Chen, H.-W. Tsaur, and C.-C. Yang, in *Molten Salts XII,"* P. C. Trulove, H. C. De Long, G. R. Stafford, and S. Deki, Editors, PV 99-41, p. 585, The Electrochemical Proceedings Series, Pennington, NJ (1999).
24. T. Takenaka, A. Hoshikawa, and M. Kawakami, in *Molen Salt Chemistry and Technology* (1993) M.-L. Saboungi and H. Kojima, Editors, PV 93-9, p. 184, The Electrochemical Society Proceedings Series, Pennington NJ (1993).
25. B. J. Tierney, W. R. Pitner, J. A. Mitchell, C. L. Hussey, and G. R. Stafford, *J. Electrochem. Soc.*, **145**, 3110 (1998).
26. X. H. Xu and C. L. Hussey, *J. Electrochem. Soc.*, **140**, 1226 (1993).
27. L. J. Durney, *Electroplating Engineering Handbook*, Van Nostrand Reinhold Co., New York (1984).
28. A. J. Dent, K. R. Seddon, and T. Welton, *J. Chem. Soc. Chem. Commun.*, **1990**, 315 (1990).
29. M. Soerlie and H. A. Oeye, *Inorg. Chem.*, **20**, 1384 (1981).
30. G. R. Stafford and T. P. Moffat, *J. Electrochem. Soc.*, **142**, 3288 (1995).
31. J. Brynestad, S. Von Winbush, H. L. Yakel, and G. P. Smith, *Inorg. Nucl. Chem. Lett.*, **6**, 889 (1970).
32. A. A. Fannin, Jr., D. A. Floreani, L. A. King, J. S. Landers, B. J. Piersma, D. J. Stech, R. L. Vaughn, J. S. Wilkes, and L. J. Williams, *J. Phys. Chem.*, **88**, 2614 (1984).
33. G. R. Stafford, L. A. Bendersky, and G. M. Janowski, Editors, *Defect Structure, Morphology, and Properties of Vapor and Electrodeposits*, The Mineral, Metals and Materials Society, Warrendale, PA (1984).
34. D. K. Smith, M. C. Nichols, and M. E. Zolensky, *A Fortran IV Program for Calculating X-Ray Powder Diffraction Patterns-Version 10*, Department of Geosciences, The Pennsylvania State University, University Park, PA (1983).
35. W. J. Boettinger, L. A. Bendersky, J. A. Cline, J. A. West, and M. J. Aziz, *Mater. Sci. Eng., A*, **133**, 592 (1991).
36. D. A. Porter and K. E. Easterling, *Phase Transformations in Metals and Alloys*, Van Nostrand Reinhold, Co, Ltd., Berkshire, UK (1981).
37. T. P. Moffat, G. R. Stafford, and D. E. Hall, *J. Electrochem. Soc.*, **140**, 2779 (1993).

Downloaded on 2012-10-05 to IP 128.143.23.241 address. Redistribution subject to ECS license or copyright; see www.esltbd.org